Scientia Iranica C (2022) 29(3), 1410–1426

Sharif University of Technology
Scientia Iranica
Transactions C: Chemistry and Chemical Engineering
http://scientiairanica.sharif.edu

Dynamic modeling and optimal control of stone-carving robotic manipulators

F. Yin[a,b,*] and W. Yan[a,b]

a. *National & Local Joint Engineering Research Center for Intelligent Manufacturing Technology of Brittle Material Products, Huaqiao University, Xiamen 361021, China.*
b. *Institute of Manufacturing Engineering, Huaqiao University, Xiamen 361021, China.*

Received 2 September 2020; received in revised form 26 September 2021; accepted 20 December 2021

KEYWORDS
Stone-carving robotic manipulators;
Dynamic modeling;
Inverse linear quadratic;
Joint angle/torque control.

Abstract. This study introduced the Inverse Linear Quadratic (ILQ) theory into the Stone-Carving Robotic Manipulators (SCRM) control system. First, the dynamic equation and state-space equation of the SCRM system were deduced with the Lagrange method. Then, the ILQ theory was employed to achieve the desired closed-loop poles assignment of the system. To simplify the design process and meet the requirement of practical use, the state feedback optimal control law was determined by an improved ILQ design method. The proposed control scheme had an explicit capacity to achieve the desired joint angle and joint torque control performances, with fewer external disturbances and no sensitivity to changing model parameters. The effectiveness of the proposed control scheme compared to traditional control strategies is shown in the simulation results. Thus, the vibration of the joint torque during the manufacturing process can be greatly reduced.

1. Introduction

Stone-carving products have become stone products with high economic value added because of its whole shape, complicated outline, and multiple carved surfaces, as shown in Figure 1. In recent years, intelligent machining equipment, such as robots, can often replace manual labor to a great extent, reduce labor costs, and simultaneously complete processing operations in various complex environments. This equipment overcomes the drawbacks of small processing range, such as no machining capability, to create huge or super-huge sculptures and inadequate postures of machining to apply industrial robots to stone carving, which is the future advancement direction of stone-carving processing [1]. Andersson and Johansson, from Linkoping University, used industrial robots in the field of wood-carving, which was the beginning of the use of industrial robots in carving processing [2]. Yin et al., from Hua Qiao University, studied stone carving by robots and performed an analysis of rough machining and finish machining of special-shaped stones [3,4].

In carving natural stones using Stone-Carving Robotic Mainpulator (SCRM) systems, as shown in Figure 2, the uncertainty of dynamics parameters and large external disturbances significantly challenge the control system design. Moreover, workpiece deformation and differences in surface quality are obtained from the complicated and variable outlines of stone-carving products caused by weak rigidity in many detailed structures and the motion performance defects while processing metal workpieces by robots. The reduced

*. *Corresponding author. Tel.: +86-18159284929*
E-mail addresses: yfc_ral@163.com (F. Yin); 1552444982@qq.com (W. Yan)

doi: 10.24200/sci.2021.56702.4866

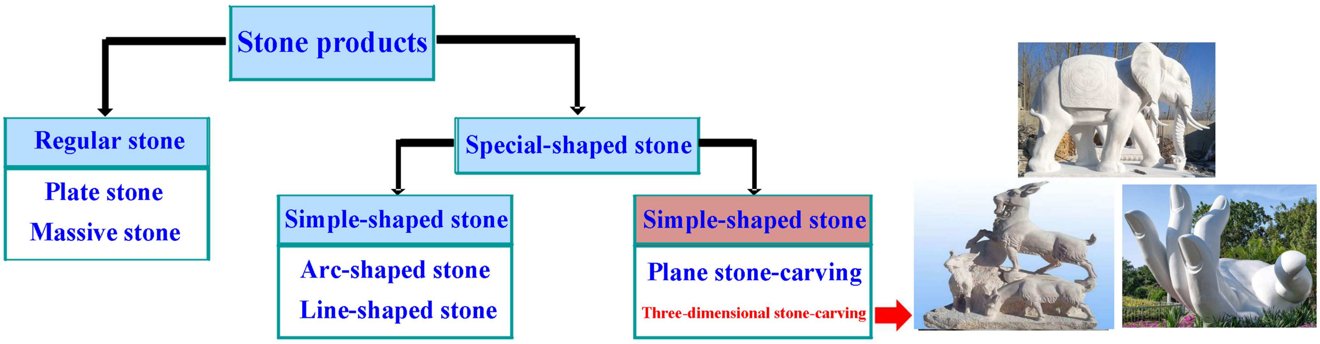

Figure 1. Main classification of stone products and stone-carving products of various materials.

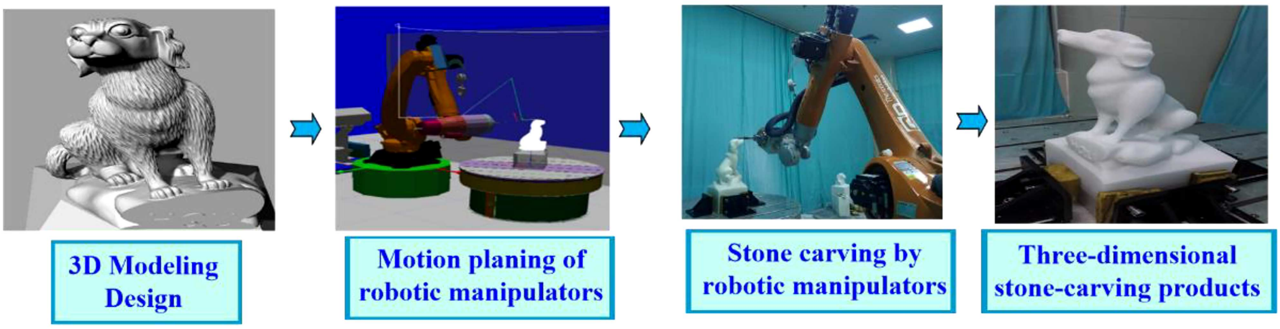

Figure 2. Machining process of SCRM.

dynamic performance of SCRM system will directly lead to unstable machining processes and even, the breakage of some detailed structures in stone-carving products owing to the hardness and brittleness of natural stones. As a result, the issue of how to realize the high-precision and strongly robust motion control of SCRM systems has turn into a technical challenge for robots' promotion and their application to the stone-carving industry.

2. Literature review

As a fundamental subject, the motion control of industrial robots has attracted much attention of scholars at both home and abroad. Industrial robots were conventionally controlled by linear PID, which had the main factures of control simplicity and ease of achievement, but required high power consumption to govern in the case of large inertia changes and could only ensure local stability [5,6]. Then, experts presented nonlinear PID control, fuzzy PID control, and neural network PID control to improve some control properties in contrast to traditional linear PID control. Su et al. devised a nonlinear PID control strategy that boosted the dynamic response of industrial robots upon designing nonlinear functions to approximate the nonlinear gain [7]. Van et al. put forward an industrial robot control system based on fuzzy PID strategy, in which the control strategy was upgraded by designing fuzzy gain parameters to improve the adaptability of the system to parameter variation [8]. Nohooji et al. applied a neural adaptive PID control strategy to an industrial robot control system and repeatedly adjusted and perfected the PID parameters using a neural network, thus learning the system's characteristic information to realize the system's compensation characteristics and improve control precision [9]. However, the control precision of the control strategies described above has a sizeable requirement for dynamic model accuracy and the dynamic model parameters of SCRM systems are immensely impacted by external loads or uncertain disturbance, resulting in difficulty attaining precise model parameters.

In order to further improve the motion performance of industrial robots, detect the uncertainty of controlled objects online, and offset the influence of uncertain external disturbances to achieve optimal control, the adaptive control algorithm and auto disturbance rejection control algorithm are both widely utilized in the field of motion control for industrial robots [10–13]. Li et al. devised a new kind of adaptive Dynamic Surface Control (DSC) method to overcome parametric uncertainties of robots; the method used does not need any support from Neural Network and is simpler and faster in calculation than other adaptive methods [14]. He et al. established an adaptive neural network controller and an industrial robot control structure with full-state feedback and output feedback while having considered the input dead-zone simulation, input saturation, and uncertain factors of dynamic models to achieve the semi-global asymptotic stability of signal [15]. With the goal of addressing the uncertain disturbance problem, Chen and Jiao built an uncertain model of a system with the help of a multilayer neural network and achieved adaptive control coupled with good trajectory tracking for industrial robots [16]. Having employed the state observer (ESO) of auto disturbance rejection control, Sanjay and others estimated the uncertain disturbances to which robots were subject to and then, discussed the issues of effectiveness and applicability of ESO [17]. Liu et al. developed research on multi-degree-of-freedom SCARA robots and the research suggested that ADRC controllers could attain good control accuracy without prior information from a dynamic model [18]. To sum up, the adaptive control algorithm and auto disturbance rejection control vary in structure; however, from the viewpoint of practical applications of SCRM systems, on the one side, real-time control in applications cannot be guaranteed for large amounts of calculations in online identification of system parameters; on the other side, fast convergence may not occur in the prediction of system parameters and the stability of the control system is difficult to ensure in case controlled model parameters mutate or larger external disturbances exist.

Linear Quadratic (LQ) optimal control is designed to seek optimal control functions that can satisfy certain constraint conditions, facilitate objective functions to obtain extremes, and achieve closed-loop optimal control by state feedback [19]. The LQ control strategy has been successfully applied to motion control systems of industrial robots, but how to choose the weighted matrix for an LQ control strategy requires much experience and extensive use of cut-and-try approach, given that they are not intuitive and are hard to tune on site [20]. Inverse Linear Quadratic (ILQ) is the inverse problem of LQ. According to the desired dynamics and steady performance index of a system, ILQ control is regarded as an efficient control strategy since it guarantees optimum performance following the selection of suitable control gains. The state feedback control was imported into the system to obtain the best control effect [21,22]. ILQ theory was successfully applied to the field of industrial control. Xu et al. presented the structural and mathematical model of an optimal current control variable speed system of a permanent magnet synchronous motor by the ILQ design method and the stability and tracking capacity were analyzed [23]. Hu et al. published a study on the application of ILQ technology in a multivariable system to tandem cold rolling. They discussed in detail the control effect that their self-devised control system had on every state variable [24]. In this paper, the SCRM control system was designed based on ILQ theory to realize the control for joint angle and joint torque with better anti-interference capacity and better dynamic control performance.

This paper is organized as follows: Section 2 describes the structure and mechanics of the SCRM system. Section 3 establishes the state space model of the SCRM system with field-obtained data. Section 4 proposes the control scheme based on ILQ theory. Section 4 compares the control performances of the ILQ control scheme with those of traditional PID control strategies. Section 5 presents conclusions.

3. Characteristics and mechanical design of SCRM

3.1. Structure of KUKA240-2900 robot manipulators

The SCRM system studied in this paper is mainly based on the KR240-R2900 robot produced by KUKA company in Germany. This robot is widely used in various industrial processes due to its high structural strength, large load, and high pose accuracy. Since all joint axes are rotating pairs, D-H parameters are used to establish the coordinate system of each link rod of the KR240-R2900 robot, as shown in Figure 3. The

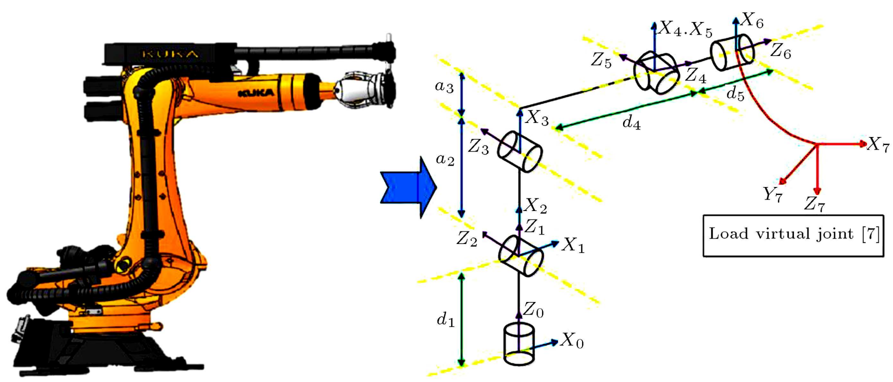

Figure 3. Important aspects of KUKA240-2900 robot.

Table 1. KR240-R2900 robot D-H parameters.

i	θ_i (°)	α_i (°)	a_i (mm)	d_i (mm)
1	$\theta 1$	0	0	675
2	$\theta 2$	–90	350	0
3	$\theta 3$	0	1350	0
4	$\theta 4$	–90	–41	1200
5	$\theta 5$	90	0	0
6	$\theta 6$	90	0	0
7	90	–90	–360	–470

virtual joint coordinate system of Joint 7 created in this paper coincides with the wrist coordinate system of Joint 6, which is used to calibrate the parameters of electric spindle and load friction parameters. Morerover, the parameters of the link rods established are shown in Table 1.

The flange end of the KR240-R2900 robot can load weights of 90 to 300 kg, and the rotation angle range and maximum movement speed of each joint are shown in Table 2. In addition, the robot can perceive the change of external torque to prevent collision. The sixth axis of the robot can rotate by 370°, while most other industrial robots can only rotate by 360°, and the work range of this robot is from 2500 to 3900 mm. The robot is characterized by large processing load, high flexibility, wide processing range, and better precision of repetitive positioning, thus meeting the requirements for carving large-sized three-dimensional stones.

3.2. Development of the SCRM machining system

The overall structure of the SCRM system is shown in Figure 4, which is mainly composed of an industrial robot body and its controller, a workpiece rotating platform (diameter 1.5 m), a carving end effector (30 kg, 22 kW), a carving tool magazine system, a water-cooling system, and the corresponding software control system. The workpiece rotating platform can move as the seventh axis of the six degrees of freedom industrial robot along a certain direction, thus expanding the

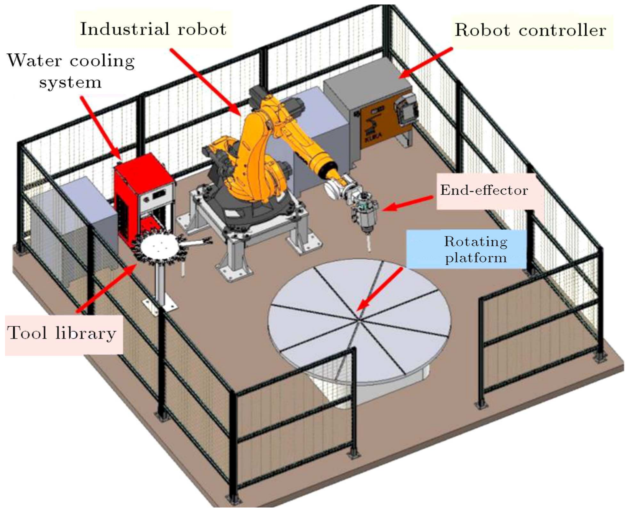

Figure 4. The overall structure of the SCRM processing system.

reachability of the SCRM system and making the carving tasks of the SCRM system easy/convenient in different areas. The end effector is the power device running at a high speed and is used to complete the carving. It is installed at the end of the robot through the fast change flange and it reaches the designated processing position along with the robot movement to complete the carving task. The engraving tool magazine system can realize automatic tool changing and storage in the processing of the SCRM system to speed up the processing rhythm.

The main function of the SCRM automatic control system is to integrate the control, signal acquisition, and processing and to safeguard the robot body, carving end effector, and other peripheral devices into an integrated system that can meet all the technological requirements of automatic carving according to the functional requirements of robot carving. The main functions of the SCRM automatic control are as follows: communication with the robot control system, data transmission between the control computer and the robot, movement control of the workpiece rotating platform, and movement control of the industrial robot body and carving end effector. This paper mainly

Table 2. Range of changes in joint axes and joint speed of KR240-R2900 robot.

Axis movement	Working range (°)	Maximum speed (°/s)
Axis 1 rotation	±185	105
Axis 2 arm	$-140 \sim -5$	101
Axis 3 arm	$-120 \sim 155$	107
Axis 4 wrist	±350	136
Axis 5 bend	±122.5	129
Axis 6 turn	±350	206

solves the problem of high-precision motion control of the industrial robot body and the carving end effector.

4. Dynamic modeling of the SCRM

In the dynamic equation of the SCRM system, the input is the angle variable quantity of each joint in the process of motion, calculated based on the moment of force of each joint, which is greatly affected by the motion characteristics of the mechanism; the motion and driving ranges of each joint are limited. In this section, combined with the entity model of the SCRM system, the Lagrange equation method is selected to derive the dynamic equation of the SCRM system and the state space model is then established.

4.1. Solution of the dynamic equation of the SCRM system

According to the definition of the Lagrange function L, the difference between the kinetic energy Ek and the potential energy Ep of the system is L such that [25]:

$$L = Ek - Ep. \tag{1}$$

According to the function L, the joint dynamic equation of the robotic manipulator is:

$$Q_i = \frac{d}{dt}\left(\frac{\partial L}{\partial \dot{q}_i}\right) - \left(\frac{\partial L}{\partial q_i}\right) \qquad i = 1, 2, 3, ..., n, \tag{2}$$

where n is the number of members of the mechanical arm, q_i the generalized coordinate of the mechanical arm, $\dot{q}_i$ the generalized speed of the mechanical arm, and Q_i the generalized force or moment of force on the ith joint of the mechanical arm.

To establish the dynamic equation of the SCRM system, the kinetic energy and potential energy of the SCRM system need to be obtained using a defined generalized coordinate system, from which the displacement variation of the position point of the joint center of gravity can be obtained and the kinetic energy required for the joint displacement change can be calculated. As shown in Figure 5, the bar model diagram of the SCRM system in the basic coordinate system is given and the small black point on the bar model is the position point of the bar center of gravity. Joints 1, 4, and 6 rotate left and right around their own members as rotation axes, with rotation radii of r_1, r_4, and r_6. Joints 2, 3, and 5 rotate around the rotation axis that is vertical to their own members, with up and down pitching motions. If the electric spindle is used as a fixed shaft that cannot rotate and is installed vertically at the 6-axis, there is $q_7 \equiv \dot{q}_7 \equiv \ddot{q}_7 \equiv 0$, $Q_7 \equiv 0$, whose length is l_7 and whose mass is m_7. Each member of the carving robot is idealized as a rigid body with uniform mass distribution and the center of gravity of each member is idealized as the midpoint of the members. The length of each member is $l_1 - l_6$ and the mass is $m_1 - m_6$.

According to the joint model in the base coordinate system, the expression of the barycenter of each member in the base coordinate system can be obtained by calculating the geometric triangle [26] as shown in Box I.

The kinetic energy of each joint is divided into

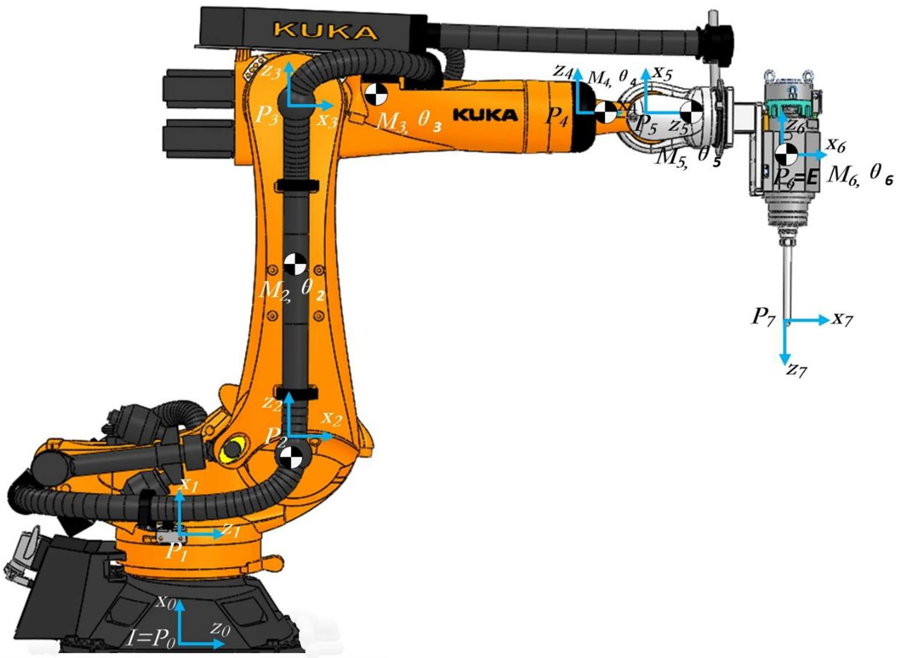

Figure 5. Schematic of the coordinate systems, joints, joint angles, and centers of mass of the SCRM system.

$$\begin{cases} x_1 = 0 \\ y_1 = 0 \\ z_1 = \frac{1}{2} l_1 \end{cases} \quad \begin{cases} x_2 = l_2 c_1 + \frac{1}{2} l_3 c_1 c_2 \\ y_2 = l_2 s_1 + \frac{1}{2} l_3 c_2 s_1 \\ z_2 = l_1 - \frac{1}{2} l_3 s_2 \end{cases} \quad \begin{cases} x_3 = l_2 c_{12} - \frac{1}{2} l_4 c_1 s_{23} + a_1 c_1 c_{23} + l_3 c_1 c_2 \\ y_3 = l_2 s_1 - \frac{1}{2} l_4 s_1 s_{23} + a_1 s_1 c_{23} + l_3 c_2 s_1 \\ z_3 = l_1 - a_1 s_{23} - \frac{1}{2} l_4 c_{23} - l_3 s_2 \end{cases}$$

$$\begin{cases} x_4 = l_2 c_1 - c_1 s_{23} \left(l_4 + \frac{1}{2} l_5 \right) + a_1 c_1 c_{23} + l_3 c_1 c_2 \\ y_4 = l_2 s_1 - s_1 s_{23} \left(l_4 + \frac{1}{2} l_5 \right) + a_1 s_1 c_{23} + l_3 c_2 s_1 \\ z_4 = l_1 - a_1 s_{23} - c_{23} \left(l_4 + \frac{1}{2} l_5 \right) - l_3 s_2 \end{cases} \quad \begin{cases} x_5 = l_2 c_1 - (l_4 + l_5) c_1 s_{23} + a_1 c_1 c_{23} + l_3 c_1 c_2 \\ y_5 = l_2 s_1 + a_1 s_1 c_{23} - (l_4 + l_5) s_1 s_{23} + l_3 c_2 s_1 \\ z_5 = l_1 - (l_4 + l_5) c_{23} - a_1 s_{23} - l_3 s_2 \end{cases}$$

$$\begin{cases} x_6 = l_2 c_1 - (l_4 + l_5) c_1 s_{23} + \left(l_6 + \frac{1}{2} l_7 \right) \left[s_5 \left(s_1 s_4 + c_4 c_1 c_{23} \right) + c_5 c_1 s_{23} \right] + a_1 c_1 c_{23} + l_3 c_1 c_2 \\ y_6 = l_2 s_1 + a_1 s_1 c_{23} - (l_4 + l_5) s_1 s_{23} - \left(l_6 + \frac{1}{2} l_7 \right) \left[s_5 \left(c_1 s_4 - c_4 s_1 c_{23} \right) - c_5 s_1 s_{23} \right] + l_3 c_2 s_1 \\ z_6 = l_1 - (l_4 + l_5) c_{23} - a_1 s_{23} + \left(l_6 + \frac{1}{2} l_7 \right) \left(c_5 c_{23} - c_4 s_5 s_{23} \right) - l_3 s_2 \end{cases}$$

Box I

the kinetic energy selected by itself and the kinetic energy causing the change of displacement of the center of gravity. By making a derivation from the formula above, the kinetic energy of each joint's center of mass can be solved through the following formula:

$$\begin{cases} Ek_1 = \frac{1}{2} m_1 \left[\left(\frac{dx_1}{dt} \right)^2 + \left(\frac{dy_1}{dt} \right)^2 + \left(\frac{dz_1}{dt} \right)^2 \right] + \frac{1}{4} m_1 r_1^2 \dot{\theta}_1^2 \\ Ek_2 = \frac{1}{2} m_2 \left[\left(\frac{dx_2}{dt} \right)^2 + \left(\frac{dy_2}{dt} \right)^2 + \left(\frac{dz_2}{dt} \right)^2 \right] + \frac{1}{6} m_2 l_2^2 \dot{\theta}_2^2 \\ Ek_3 = \frac{1}{2} m_3 \left[\left(\frac{dx_3}{dt} \right)^2 + \left(\frac{dy_3}{dt} \right)^2 + \left(\frac{dz_3}{dt} \right)^2 \right] + \frac{1}{6} m_3 l_3^2 \dot{\theta}_3^2 \\ Ek_4 = \frac{1}{2} m_4 \left[\left(\frac{dx_4}{dt} \right)^2 + \left(\frac{dy_4}{dt} \right)^2 + \left(\frac{dz_4}{dt} \right)^2 \right] + \frac{1}{4} m_4 r_4^2 \dot{\theta}_4^2 \\ Ek_5 = \frac{1}{2} m_5 \left[\left(\frac{dx_5}{dt} \right)^2 + \left(\frac{dy_5}{dt} \right)^2 + \left(\frac{dz_5}{dt} \right)^2 \right] + \frac{1}{6} m_5 l_5^2 \dot{\theta}_5^2 \\ Ek_6 = \frac{1}{2} m_6 \left[\left(\frac{dx_5}{dt} \right)^2 + \left(\frac{dy_5}{dt} \right)^2 + \left(\frac{dz_5}{dt} \right)^2 \right] \\ \qquad + \frac{1}{4} m_6 \left(r_6 + \frac{1}{2} l_7 \right)^2 \dot{\theta}_6^2 \end{cases} \tag{3}$$

The total kinetic energy of the SCRM system is obtained as follows:

$$Ek = Ek_1 + Ek_2 + Ek_3 + Ek_4 + Ek_5 + Ek_6. \tag{4}$$

The total potential energy of the SCRM system is obtained as follows:

$$\begin{aligned} Ep &= Ep_1 + Ep_2 + Ep_3 + Ep_4 + Ep_5 + Ep_6 \\ &= mgz_1 + mgz_2 + mgz_3 + mgz_4 + mgz_5 \\ &+ mgz_6 \end{aligned} \tag{5}$$

The functional relationship of the SCRM system in a Cartesian space is consistent with that in the joint space. The functional relationship is expressed by performing a dot-multiplication between the external force spinor F in Cartesian space and the vector change $\boldsymbol{\Delta X}$ of displacement of the carving cutter head at the end:

$$\mathbf{F} \Delta \mathbf{X} = \tilde{\mathbf{Q}} \Delta \mathbf{q}, \tag{6}$$

where $\tilde{Q}$ is the disturbing moment of each joint under the action of F and $\boldsymbol{\Delta q}$ is the angle variation of each joint under the action of the external force spinor.

According to the definition of Jacobian matrix (Eq. (7)), Eq. (8) is obtained:

$$\mathbf{J}(\mathbf{q}) = \frac{\Delta \mathbf{X}}{\Delta \mathbf{q}}, \tag{7}$$

$$\tilde{\mathbf{Q}} = \mathbf{J}(\mathbf{q})^T \mathbf{F}. \tag{8}$$

The total kinetic energy and potential energy of the SCRM system obtained are substituted into Eq. (2); the disturbing moment $\tilde{\mathbf{Q}}$ of the SCRM system in Cartesian space is considered; and the moment acting on each joint can be obtained and expressed as the matrix:

$$\mathbf{Q} = \mathbf{M}(\mathbf{q}) \ddot{\mathbf{q}} + \mathbf{C}(\mathbf{q}, \dot{\mathbf{q}}) \dot{\mathbf{q}} + \mathbf{G}(\mathbf{q}) + \mathbf{J}(\mathbf{q})^T \mathbf{F}, \tag{9}$$

where $\mathbf{Q}$ is the driving moment vector of each joint, $\mathbf{q}$ the position vector of each joint, $\dot{\mathbf{q}}$ the velocity vector of each joint, $\ddot{\mathbf{q}}$ the acceleration vector of each joint, $\mathbf{M(q)}$ the inertia matrix of joint space, $\mathbf{C}(\mathbf{q}, \dot{\mathbf{q}})$ the Coriolis force matrix and centripetal force matrix, $\mathbf{G(q)}$ the gravity load matrix, and $\mathbf{J(q)}$ the Jacobian matrix of the SCRM system.

4.2. State space model

The overall nonlinear mathematic model for the SCRM system can be obtained using Eq. (6). The system is linearized about the setup value with Taylor's series expansion. As a result, the state space representation of the system can be expressed by:

$$\begin{cases} \dot{\mathbf{x}}(t) = \mathbf{A}\mathbf{x}(t) + \mathbf{B}\mathbf{u}(t) + \mathbf{D}\mathbf{d}(t) \\ \mathbf{y}(t) = \mathbf{C}\mathbf{x}(t) \end{cases} \tag{10}$$

where:

$$\mathbf{y}(t) = [\Delta \mathbf{q}] = \left[\Delta\theta_1 \quad \Delta\theta_2 \quad \Delta\theta_3 \quad \Delta\theta_4 \quad \Delta\theta_5 \quad \Delta\theta_6 \right]^{\mathrm{T}},$$

Table 3. Dynamic characteristic parameters of all components of SCRM.

Axis movement	**Link mass/kg**	**Center of mass/m (base coordinate frame)**			**Moment of inertial/kgm^2 (center of mass coordinate frame)**		
		z	y	x	I_{zz}	I_{yy}	I_{xx}
Axis 1	138.8	0.07	0.37	0.08	5.24	5.04	1.73
Axis 2	94.72	0.19	0.79	0.23	4.76	4.71	0.51
Axis 3	32.61	0.21	1.18	0.07	1.05	0.97	0.17
Axis 4	27.95	0.69	1.20	0.04	0.29	0.29	6.16
Axis 5	13.48	0.88	1.21	0.03	9.33	7.01	4.88
Axis 6	0.332	0.98	1.23	0.03	2.17	1.13	1.13

$$\mathbf{x}(t)=\begin{bmatrix}\Delta\mathbf{q} & \Delta\dot{\mathbf{q}}\end{bmatrix}=\begin{bmatrix}\Delta\theta_1 & \Delta\theta_2 & \Delta\theta_3 & \Delta\theta_4 & \Delta\theta_5 & \Delta\theta_6 & \Delta\dot{\theta}_1 & \Delta\dot{\theta}_2 & \Delta\dot{\theta}_3 & \Delta\dot{\theta}_4 & \Delta\dot{\theta}_5 & \Delta\dot{\theta}_6\end{bmatrix}^{\mathrm{T}},$$

$$\mathbf{u}(t)=[\Delta\mathbf{Q}]=\begin{bmatrix}\Delta Q_1 & \Delta Q_2 & \Delta Q_3 & \Delta Q_4 & \Delta Q_5 & \Delta Q_6\end{bmatrix}^{\mathrm{T}},$$

$$\mathbf{d}(t)=[\Delta\mathbf{F}]=\begin{bmatrix}\Delta f_x & \Delta f_y & \Delta f_z & \Delta\tau_x & \Delta\tau_y & \Delta\tau_z\end{bmatrix}^{\mathrm{T}}.$$

The coefficient matrix satisfies the following form ($\mathbf{O}$ is the zero matrix; $\mathbf{I}$ is the unit matrix):

$$\mathbf{A}=\begin{bmatrix}\mathbf{O}_{6\times6} & \mathbf{I}_{6\times6}\\ \left(-\mathbf{M}^{-1}\mathbf{G}\mathbf{q}^{-1}\right)_{6\times6} & \left(-\mathbf{M}^{-1}\mathbf{C}\right)_{6\times6}\end{bmatrix}_{12\times12},$$

$$\mathbf{B}=\begin{bmatrix}\mathbf{O}_{6\times6}\\ \left(\mathbf{M}^{-1}\right)_{6\times6}\end{bmatrix}_{12\times6},\qquad \mathbf{C}=\begin{bmatrix}\mathbf{I}_{6\times6}\\ \mathbf{O}_{6\times6}\end{bmatrix}^{\mathrm{T}}_{6\times12}$$

$$\mathbf{D}=\begin{bmatrix}\mathbf{O}_{6\times6}\\ \left(-\mathbf{M}^{-1}\mathbf{J}^{\mathrm{T}}\right)_{6\times6}\end{bmatrix}_{12\times6}.$$

Table 3 lists the dynamic characteristic parameters of the SCRM system. This table contains information such as weight, and moment of inertia around the center of mass of each link, and the center of mass of each link relative to the reference coordinate system.

5. Controller design for SCRM based on ILQ theory

5.1. ILQ design theory

The inverse problem of the LQ regulator (ILQ) was proposed by Kalman. In the design process of LQ, the weighting matrix $\mathbf{Q}, \mathbf{R}$ is determined first and the optimal feedback $\mathbf{K}$ is then determined [27]. However, in the design process of ILQ, the optimal and stable feedback control rate $\mathbf{K}$ is solved first, and the corresponding weighting matrix $\mathbf{Q}, \mathbf{R}$ and solution of Riccati equation are then determined.

First, consider the following system matrix $\mathbf{A}$ and input matrix $\mathbf{B}$:

$$\mathbf{A}=\begin{bmatrix}\mathbf{A}_{11} & \mathbf{A}_{12}\\ \mathbf{A}_{21} & \mathbf{A}_{22}\end{bmatrix}\qquad \mathbf{B}=\begin{bmatrix}\mathbf{0}\\ \mathbf{I}\end{bmatrix}, \tag{11}$$

where $\mathbf{A}\in\mathbf{R}^{n\times n}$, $\mathbf{A}_{11}\in\mathbf{R}^{(n-m)\times(n-m)}$ and $\mathbf{A}_{22}\in\mathbf{R}^{m\times m}$; $\mathbf{I}$ is the unit matrix of $\mathbf{R}^{m\times m}$.

Let the optimal stable feedback control rate $\mathbf{K}$ have the following form:

$$\mathbf{K}=\begin{bmatrix}\mathbf{K}_1 & \mathbf{K}_2\end{bmatrix}, \tag{12}$$

where $\mathbf{K}_1\in\mathbf{R}^{(n-m)\times m}$, $\mathbf{K}_2\in\mathbf{R}^{m\times m}$. Defining:

$$\mathbf{V}=[v_1, v_2, \cdots, v_m]^T,$$

$$\mathbf{\Sigma}=diag\left(\sigma_1, \sigma_2, \cdots, \sigma_m\right),$$

and letting:

$$rank(\mathbf{KB})=rank(\mathbf{B}),$$

the following relational function can be obtained:

$$\mathbf{KB}=\mathbf{K}_2=\mathbf{V}^{-1}\mathbf{\Sigma}\mathbf{V}. \tag{13}$$

Then, the column vectors of $\mathbf{K_2}$ constitute the maximum linear independence group of $\mathbf{KB}$ so that $\mathbf{K}_1$ can be expressed as follows:

$$\mathbf{K}_1=\mathbf{K}_2\mathbf{F}_1. \tag{14}$$

In conclusion, in the row full rank matrix $\mathbf{B}$, the optimal control rate $\mathbf{K}$ can be expressed as follows:

$$\mathbf{K}=\mathbf{V}^{-1}\mathbf{\Sigma}\mathbf{V}\left[\mathbf{F}_1, \mathbf{I}\right], \tag{15}$$

$$\mathbf{H}=\mathbf{BK}/2-\mathbf{A}=\begin{bmatrix}-\mathbf{A}_{11} & -\mathbf{A}_{12}\\ \mathbf{V}^{-1}\sum\mathbf{V}\mathbf{F}_1-\mathbf{A}_{21} & \mathbf{V}^{-1}\sum\mathbf{V}\mathbf{F}_1-\mathbf{A}_{22}\end{bmatrix}. \tag{16}$$

Therefore, as long as the nonsingular matrix is $\mathbf{V}$, $\sum > \mathbf{0}$ and the real matrix $\mathbf{F_1}$ are properly selected to make $\mathbf{H} \geq \mathbf{0}$ shown in Eq. (16); such $\mathbf{K}$ must be optimal and stable.

For the system matrix $\mathbf{A}$ and input matrix $\mathbf{B}$ shown in Eq. (16), the following relationship is established:

$$(\mathbf{A}_{11} - \mathbf{A}_{12}\mathbf{F}_1)\mathbf{T}_1 = \mathbf{T}_1\mathbf{S}, \tag{17}$$

$$\mathbf{S} = (block)diag(\mathbf{s}_1, \cdots, \mathbf{s}_{n-m}). \tag{18}$$

If there is a conjugate complex root, $\mathbf{S_i}$ is expressed as follows:

$$\mathbf{s}_i = \begin{bmatrix} \mathrm{Re}(\mathbf{s}_i) & \mathrm{Im}(\mathbf{s}_i) \\ -\mathrm{Im}(\mathbf{s}_i) & \mathrm{Re}(\mathbf{s}_i) \end{bmatrix}. \tag{19}$$

Then, we have:

$$\mathbf{G} = -\mathbf{F}_1\mathbf{T}_1. \tag{20}$$

According to $\mathbf{VT}_1$ and $\mathbf{G}$ above and related control laws, the following transformation matrix can be defined:

$$\mathbf{T} = \begin{bmatrix} \mathbf{T}_1 & \mathbf{0} \\ \mathbf{G} & \mathbf{V}^{-1} \end{bmatrix}. \tag{21}$$

The matrix $\mathbf{AF} = \mathbf{A} - \mathbf{BKH} = \mathbf{BK}/2 - \mathbf{A}$ is transformed as follows:

$$\bar{\mathbf{A}} = \mathbf{T}^{-1}\mathbf{AT} = \begin{bmatrix} \mathbf{S} & \bar{\mathbf{A}}_{12} \\ \bar{\mathbf{A}}_{21} & \bar{\mathbf{A}}_{22} \end{bmatrix}, \tag{22}$$

$$\bar{\mathbf{F}} = \mathbf{T}^{-1}\mathbf{FT} = \begin{bmatrix} \mathbf{S} & \bar{\mathbf{A}}_{12} \\ \bar{\mathbf{A}}_{21} & \bar{\mathbf{A}}_{22} - \mathbf{\Sigma} \end{bmatrix}, \tag{23}$$

$$\bar{\mathbf{H}} = \mathbf{T}^{-1}\mathbf{HT} = \begin{bmatrix} -\mathbf{S} & -\bar{\mathbf{A}}_{12} \\ -\bar{\mathbf{A}}_{21} & -\bar{\mathbf{A}}_{22} + \mathbf{\Sigma}/2 \end{bmatrix}, \tag{24}$$

where $\bar{\mathbf{A}}_{12} = \mathbf{T}^{-1}\mathbf{A}_{12}\mathbf{V}^{-1}$, $\bar{\mathbf{A}}_{21} = \mathbf{V}(\mathbf{A}_{21}\mathbf{T}_1 + \mathbf{A}_{22}\mathbf{G} - \mathbf{GS})$, $\bar{\mathbf{A}}_{22} = \mathbf{V}(\mathbf{A}_{22} + \mathbf{F}_1\mathbf{A}_{21})\mathbf{V}^{-1}$.

The detailed calculation process of key parameter is described as follows:

(a) *Calculation method of $\boldsymbol{F_1}$*. Let $\mathbf{T}_1 = [t_1, t_2, \cdots, t_{n-m}]$ and $\mathbf{G} = [g_1, g_2, \cdots, g_{n-m}]$; select arbitrary pole $\{\mathbf{s}_i\}$ and vector $\{\mathbf{g}_i\}$. The following relationship can be obtained from Eqs. (17) and (20):

$$\mathbf{A}_{11}\mathbf{t}_i + \mathbf{A}_{12}\mathbf{g}_i = \mathbf{s}_i\mathbf{t}_i \Rightarrow (\mathbf{s}_i\mathbf{I} - \mathbf{A}_{11})\mathbf{t}_i$$
$$= \mathbf{A}_{12}\mathbf{g}_i, \mathbf{s}_i \neq \lambda(\mathbf{A}_{11}), \tag{25}$$

$$\mathbf{t}_i = (\mathbf{s}_i\mathbf{I} - \mathbf{A}_{11})^{-1}\mathbf{A}_{12}\mathbf{g}_i. \tag{26}$$

If $\mathbf{T_1}$ is reversible, the following can be obtained from Eq. (20):

$$\mathbf{F}_1 = -\mathbf{G}{\mathbf{T}_1}^{-1}. \tag{27}$$

(b) *Calculation method of $\sum$. $\bar{\boldsymbol{H}}$* which is a positive semidefinite matrix can be known from Eq. (24); then, $\bar{\mathbf{H}} + \bar{\mathbf{H}}^{\mathrm{T}} > 0$:

$$\bar{\mathbf{H}} + \bar{\mathbf{H}}^{\mathrm{T}} =$$
$$\begin{bmatrix} -(\mathbf{S} + \mathbf{S}^{\mathrm{T}}) & -(\bar{\mathbf{A}}_{12} + \bar{\mathbf{A}}_{21}^{\mathrm{T}}) \\ -(\bar{\mathbf{A}}_{21} + \bar{\mathbf{A}}_{12}^{\mathrm{T}}) & \mathbf{\Sigma} - (\bar{\mathbf{A}}_{22} + \bar{\mathbf{A}}_{22}^{\mathrm{T}}) \end{bmatrix}. \tag{28}$$

Let $\mathbf{H}_A = \bar{\mathbf{H}} + \bar{\mathbf{H}}^{\mathrm{T}}$, $\mathbf{H}_{A_{12}} = -(\bar{\mathbf{A}}_{12} + \bar{\mathbf{A}}_{21}^{\mathrm{T}})$.

Then, we have:

$$\mathbf{H}_A = \begin{bmatrix} -(\mathbf{S} + \mathbf{S}^{\mathrm{T}}) & \mathbf{H}_{A_{12}} \\ \mathbf{H}_{A_{12}}^T & \mathbf{\Sigma} - (\bar{\mathbf{A}}_{22} + \bar{\mathbf{A}}_{22}^{\mathrm{T}}) \end{bmatrix}, \tag{29}$$

$$\mathbf{U} = \begin{bmatrix} \mathbf{I}_{n-m} & 0 \\ \mathbf{H}_{A_{12}}^{\mathrm{T}}(\mathbf{S} + \mathbf{S}^{\mathrm{T}})^{-1} & \mathbf{I}_m \end{bmatrix} \Rightarrow \bar{\mathbf{H}}_A$$
$$= \mathbf{U}\mathbf{H}_A\mathbf{U}^{\mathrm{T}} = \begin{bmatrix} -(\mathbf{S} + \mathbf{S}^{\mathrm{T}}) & 0 \\ 0 & \mathbf{\Sigma} - \mathbf{E} \end{bmatrix}. \tag{30}$$

Then, we have:

$$\lambda(-\mathbf{S} - \mathbf{S}^{\mathrm{T}}) > 0,$$
$$\lambda(\mathbf{\Sigma} - \mathbf{E}) > 0 \Rightarrow \bar{\mathbf{H}}_A > 0 \Rightarrow \mathbf{H}_A > 0, \tag{31}$$

where $\lambda(\bullet)$ is the eigenvalue of the matrix. The following can be obtained:

$$\bar{\mathbf{H}} + \bar{\mathbf{H}}^{\mathrm{T}} > 0, \tag{32}$$

$$\mathbf{E} = (\bar{\mathbf{A}}_{22} + \bar{\mathbf{A}}_{22}^{\mathrm{T}}) - (\bar{\mathbf{A}}_{21} + \bar{\mathbf{A}}_{12}^{\mathrm{T}})(\mathbf{S} + \mathbf{S}^{\mathrm{T}})^{-1}$$
$$(\bar{\mathbf{A}}_{12} + \bar{\mathbf{A}}_{21}^{\mathrm{T}}). \tag{33}$$

To reduce the gain, the weighting matrix $\mathbf{\Pi}$ is introduced. $\mathbf{\Pi}$ is a real diagonal matrix, which mainly assigns weight to vectors $\mathbf{G}$ and $\mathbf{T_1}$ as follows:

$$\bar{\mathbf{G}} = \mathbf{G\Pi}, \qquad \bar{\mathbf{T}}_1 = \mathbf{T}_1\mathbf{\Pi}, \tag{34}$$

$$\mathbf{\Pi} = diag(\pi_1, \pi_2, \cdots, \pi_{n-m}), \quad \forall \pi_i \neq 0. \tag{35}$$

The new state transformation matrix after weighting is as follows:

$$\bar{\mathbf{T}} = \begin{bmatrix} \mathbf{T}_1\mathbf{\Pi} & \mathbf{0} \\ \mathbf{G\Pi} & \mathbf{V}^{-1} \end{bmatrix}. \tag{36}$$

Upon substituting Eq. (36) into Eqs. (22), (23), and (24), the following can be obtained:

$$\bar{\mathbf{A}} = \mathbf{T}^{-1}\mathbf{AT} = \begin{bmatrix} \mathbf{S} & \mathbf{\Pi}^{-1}\bar{\mathbf{A}}_{12} \\ \bar{\mathbf{A}}_{21}\mathbf{\Pi} & \bar{\mathbf{A}}_{22} \end{bmatrix}, \tag{37}$$

$$\bar{\mathbf{F}} = \mathbf{T}^{-1}\mathbf{F}\mathbf{T} = \begin{bmatrix} \mathbf{S} & \mathbf{\Pi}^{-1}\bar{\mathbf{A}}_{12} \\ \bar{\mathbf{A}}_{21}\mathbf{\Pi} & \bar{\mathbf{A}}_{22} - \mathbf{\Sigma} \end{bmatrix}, \tag{38}$$

$$\bar{\mathbf{H}} = \mathbf{T}^{-1}\mathbf{H}\mathbf{T} = \begin{bmatrix} -\mathbf{S} & -\mathbf{\Pi}^{-1}\bar{\mathbf{A}}_{12} \\ -\bar{\mathbf{A}}_{21}\mathbf{\Pi} & -\bar{\mathbf{A}}_{22} + \mathbf{\Sigma}/2 \end{bmatrix}, \tag{39}$$

$$\mathbf{E} = (\bar{\mathbf{A}}_{22} + \bar{\mathbf{A}}_{22}^{\mathrm{T}}) - \left[(\mathbf{\Pi}^{-1}\bar{\mathbf{A}}_{12})^{\mathrm{T}} + \bar{\mathbf{A}}_{21}\mathbf{\Pi}\right]$$

$$(\mathbf{S} + \mathbf{S}^{\mathrm{T}})^{-1}\left[(\mathbf{\Pi}^{-1}\bar{\mathbf{A}}_{12})^{\mathrm{T}} + \bar{\mathbf{A}}_{21}\mathbf{\Pi}\right]^{\mathrm{T}}. \tag{40}$$

After introducing the weighting matrix $\mathbf{\Pi}$, the lower limit $\{\sigma_i\}$ of each diagonal element of $\sum$ needs to meet the following conditions:

$$\sigma_i > \lambda_{\max}(\bar{\mathbf{E}}). \tag{41}$$

If the weighting matrix Σ is strictly limited to $\mathbf{\Sigma} = \sigma\mathbf{\Gamma}$, $\mathbf{\Gamma} = diag(\gamma_1, \gamma_2, \cdots, \gamma_m)$, $\gamma_i > 0$, then we have:

$$\sigma_i > \lambda_{\max}(\bar{\mathbf{E}}_r), \bar{\mathbf{E}}_r = \mathbf{\Gamma}^{-1/2}\mathbf{E}\mathbf{\Gamma}^{-1/2}. \tag{42}$$

Thus far, $\sum$, $\mathbf{F_1}$ in the control rate $\mathbf{K} = \mathbf{V}^{-1}\sum\mathbf{V}\left[\mathbf{F}_1, \mathbf{I}\right]$ are determined. For simplicity, the matrix $\mathbf{V}$ is taken as the unit matrix and the control rate $\mathbf{K}$ is determined.

5.2. Controller design

According to the introduction of ILQ theory in the previous section, an important precondition for ILQ design is the form of input matrix $\mathbf{B}$. The input matrix $\mathbf{B}$ as shown in Eq. (11) exactly conforms to the form that input matrix should possess as required by ILQ design; therefore, the expected pole assignment to system $(\mathbf{A}, \mathbf{B})$ can be made based on ILQ theory; the state feedback matrix $\mathbf{K}_A$ can be obtained; and then $\mathbf{K}_F$ and $\mathbf{K}_I$ can be obtained by linear transformation [28]. The relationship between $\mathbf{K}_F$ and $\mathbf{K}$ is obtained as follows:

$$\mathbf{K} = [\mathbf{K}_F, \mathbf{K}_I] = \mathbf{K}_A\mathbf{\Gamma}^{-1}. \tag{43}$$

Furthermore, the special form of state feedback matrix $\mathbf{K}_A$ in ILQ design is considered as follows:

$$\mathbf{K}_A = \mathbf{V}^{-1}\mathbf{\Sigma}\mathbf{V}\left[\mathbf{F}_1, \mathbf{I}\right] = \mathbf{\Sigma}\left[\mathbf{F}_1, \mathbf{I}\right]. \tag{44}$$

For simplicity, let $\mathbf{V}$=$\mathbf{I}$:

$$[\mathbf{K}_{F0}, \mathbf{K}_{I0}] = [\mathbf{F}_1, \mathbf{I}]\,\mathbf{\Gamma}^{-1}. \tag{45}$$

In the common method of ILQ design, the selection of expected poles $\{s_i\}$ and degree of freedom of eigenvector $\{g_i\}$ are carried out separately, and there is no uniform method and standard for the selection of these parameters, mainly depending on a large number of "cut and try" approach attempts. Therefore, this section is concerned with the improvement of the conventional design method, mainly to optimize the selection of eigenvector $\{g_i\}$. The improvement method is as follows.

If $(\mathbf{A}, \mathbf{B})$ is fully controllable and $(\mathbf{A}, \mathbf{C})$ observable, then the system of $(\mathbf{A_{cl}}, \mathbf{B_{cl}})$ can realize arbitrary pole assignment by state feedback:

$$\mathbf{A}_A = \mathbf{\Gamma}^{-1}\mathbf{A}_{cl}\mathbf{\Gamma}, \tag{46}$$

$$\mathbf{B}_A = \mathbf{\Gamma}^{-1}\mathbf{B}_{cl}, \tag{47}$$

where:

$$\mathbf{A}_A = \begin{bmatrix} \mathbf{A} & \mathbf{B} \\ 0 & 0 \end{bmatrix}; \quad \mathbf{B}_A = \begin{bmatrix} 0 \\ \mathbf{I} \end{bmatrix}; \quad \mathbf{A}_{cl} = \begin{bmatrix} \mathbf{A} & 0 \\ \mathbf{C} & 0 \end{bmatrix};$$

$$\mathbf{B}_{cl} = \begin{bmatrix} \mathbf{B} \\ 0 \end{bmatrix}; \qquad \mathbf{\Gamma} = \begin{bmatrix} \mathbf{A} & \mathbf{B} \\ \mathbf{C} & 0 \end{bmatrix}.$$

For pole assignment to $(\mathbf{A}_{cl}, \mathbf{B}_{cl})$, the expected pole is composed of two parts: the dominant pole $\{s_i\}$ $(1 \leq i \leq n)$ and the nondominant pole $\{\gamma_i\}$ $(1 \leq i \leq m)$. In addition, the feedback matrix $\mathbf{K} = [\mathbf{K}_F, \mathbf{K}_I]$ is obtained. For pole assignment to $(\mathbf{A}_A, \mathbf{B}_A)$, the ILQ theory is use and the feedback matrix is obtained. The relationship between $\mathbf{K}$ and $\mathbf{K}_A$ is shown in Eq. (33). After adding state feedback, we have:

$$\bar{\mathbf{A}}_A = \mathbf{A}_A - \mathbf{B}_A\mathbf{K}_A, \tag{48}$$

$$\bar{\mathbf{A}}_{cl} = \mathbf{A}_{cl} - \mathbf{B}_{cl}\mathbf{K}, \tag{49}$$

$$\bar{\mathbf{A}}_A = \mathbf{\Gamma}^{-1}\mathbf{A}_{cl}\mathbf{\Gamma} - \mathbf{\Gamma}^{-1}\mathbf{B}_{cl}\mathbf{K}\mathbf{\Gamma} = \mathbf{\Gamma}^{-1}(\mathbf{A}_{cl} - \mathbf{B}_{cl}\mathbf{K})\mathbf{\Gamma}$$

$$= \mathbf{\Gamma}^{-1}\bar{\mathbf{A}}_{cl}\mathbf{\Gamma}. \tag{50}$$

Let $\{f_i\}$ be the eigenvector of eigenvalue $\{s_i\}$ of $\bar{\mathbf{A}}_{cl}$ and $\{f_{iA}\}$ be the eigenvector of eigenvalue $\{s_{iA}\}$ of $\bar{\mathbf{A}}_A$. Then, the following relationship can be established:

$$\mathbf{f}_{iA} = \mathbf{\Gamma}^{-1}\mathbf{f}_i = \begin{bmatrix} t_i \\ g_i \end{bmatrix}. \tag{51}$$

If pole assignment to $(\mathbf{A}_A, \mathbf{B}_A)$ is made based on ILQ theory, the dominant pole $\{s_i\}$ is selected as the expected pole and $\{g_i\}$ of degree of freedom matrix $\mathbf{G}$ of eigenvector assignment is determined as shown in Eq. (41). Moreover, the parameters of vector selection will be greatly simplified.

Based on the established state-space model of the SCRM system and the ILQ control algorithm, which is shown in Figure 6, the SCRM control system can be established based on the following steps:

- **Step 1:** Establish the extended state space matrix of the SCRM system:

$$\begin{cases} \dot{\mathbf{x}} = \mathrm{A}_A\mathrm{x} + \mathrm{B}_A\mathrm{u} + \mathbf{D}\mathbf{d} \\ \mathrm{y} = \mathrm{Cx} \end{cases}$$

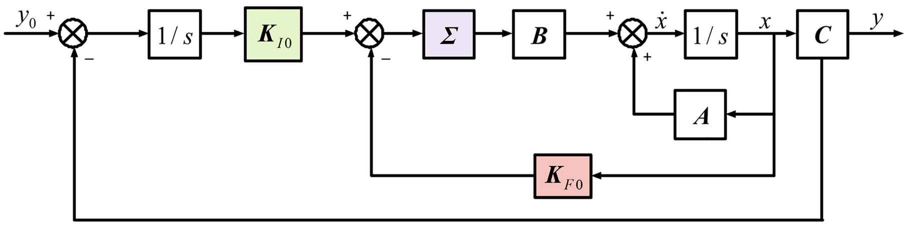

Figure 6. The structure diagram of ILQ control theory.

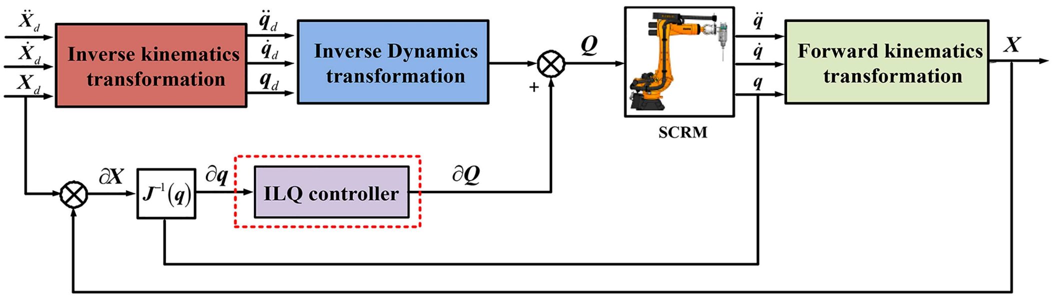

Figure 7. The structure diagram of the ILQ-based SCRM control system.

where $\mathbf{A}_A = \mathbf{\Gamma}^{-1}\mathbf{A}_{cl}\mathbf{\Gamma}$, $\mathbf{B}_A = \mathbf{\Gamma}^{-1}\mathbf{B}_{cl}\mathbf{\Gamma}$.

$$\mathbf{\Gamma} = \begin{bmatrix} \mathbf{A} & \mathbf{B} \\ \mathbf{C} & \mathbf{O}_{6\times 6} \end{bmatrix} \qquad \mathbf{A}_{cl} = \begin{bmatrix} \mathbf{A} & \mathbf{O}_{12\times 6} \\ \mathbf{C} & \mathbf{O}_{6\times 6} \end{bmatrix}$$

$$\mathbf{B}_{cl} = \begin{bmatrix} \mathbf{B} \\ \mathbf{O}_{6\times 6} \end{bmatrix}.$$

- **Step 2:** Determine the matrix $\mathbf{F_1}$. According to the expected response of each joint force of the SCRM comprehensive system, the expected dominant pole of the system is selected as follows:

$$\mathbf{s}_a = \big[-20.5 + 16.4i \quad -20.5 - 16.4i \quad -24 \quad -28$$

$$-32 \quad -36 \quad -40 \quad -44 \quad -48 \quad -52 \quad -56 \quad -60\big].$$

The nondominant pole is as follows:

$$\mathbf{s}_b = \begin{bmatrix} -90 & -100 & -110 & -120 & -130 & -140 \end{bmatrix}.$$

Constructing matrix $\mathbf{S}$ is as follows:

$$\mathbf{S} = \begin{bmatrix} \mathbf{s}_a & \mathbf{s}_b \end{bmatrix}.$$

- **Step 3:** By distributing the poles to $(\mathbf{A}_{cl}\ \mathbf{B}_{cl})$, calculating the eigenvector $\mathbf{f_i}$ corresponding to the dominant pole $\mathbf{s_a}$, and making linear coordinate transformation to eigenvector $\mathbf{f_i}$ according to Eq. (41), the equation shown in Box II is obtained.

- **Step 4:** According to the formula $\mathbf{f}_{iA} = \begin{bmatrix} \mathbf{t}_i & \mathbf{g}_i \end{bmatrix}^T$, $[\mathbf{t}_i]$ and $[\mathbf{g}_i]$ are obtained through extraction shown in Box III.

- **Step 5:** Let $V = I$ and when the weighting matrix is not introduced, the lower limit of $\sum$ diagonal element is obtained as follows:

$\sigma_i > 17345$.

- **Step 6:** According to the formula $\begin{bmatrix} \mathbf{K}_{F0} & \mathbf{K}_{I0} \end{bmatrix} = \begin{bmatrix} \mathbf{F}_1 & \mathbf{I} \end{bmatrix} \mathbf{\Gamma}^{-1}$, calculate $\mathbf{K}_{F0}$ and $\mathbf{K}_{I0}$ by the equations shown in Box IV.

6. Simulation results

Based on the above results, the SCRM system model and ILQ controller were obtained, and the structure diagram of the proposed ILQ-based robot control system is shown in Figure 7. In this simulation, the ILQ controller is compared with the PI controller based on the control performance of joint angle and joint torque. The Industrial Personal Computer (IPC) with Intel Core i7 4.6 GHz processor, 32 GB RAM is applied to run the simulation platform (MATLAB 2017a/Simulink), and the sampling time is set as 5ms in Matlab 2017a/Simulink. Moreover, the inverse kinematics transformation and forward kinematics transformation in Figure 7 are calculated with robotic toolbox for Matlab 2017a.

6.1. Step response performance comparison

During the machining process of the SCRM system, the control accuracy of the joint angle in the SCRM system directly affects the dimensional precision of the product. To compare the control accuracy of the PI controller and the ILQ controller, a step testing signal was added to the initial value of the joint angle at $t = 0.2$ s. The simulation results are shown in Figure 8.

As shown in Figure 8, the response time of the PI controller at each joint angle is approximately 0.015 s, the overshoot is approximately 2.58%, and

$$
\mathbf{f}_{iA} = \left[\begin{matrix}
4.037e-4 & 8.125e-5 & 7.065e-5 & 5.069e-4 & 0.001 & -2.920e-4 & -2.605e-4 & -5.511e-5 \\
0.002 & 2.017e-4 & 4.045e-4 & 7.469e-4 & -5.013e-4 & 2.302e-4 & -3.057e-4 & 0.001 \\
-0.001 & -7.120e-5 & 2.113e-4 & 4.870e-4 & 1.204e-4 & 2.525e-4 & 0.002 & 6.903e-5 \\
-5.352e-4 & -4.247e-4 & 9.116e-4 & 0.001 & -8.036e-4 & -9.413e-5 & -1.870e-5 & -3.909e-4 \\
-1.810e-4 & 4.715e-4 & -1.925e-5 & -0.001 & -4.309e-4 & -0.001 & 3.229e-4 & 1.036e-4 \\
-6.283e-4 & 9.783e-4 & 2.918e-4 & 7.052e-4 & -1.599e-4 & 5.019e-4 & 2.528e-5 & -4.822e-4 \\
-0.008 & -0.002 & -0.020 & -0.011 & -0.033 & 0.008 & 0.007 & 0.001 \\
-0.034 & -0.006 & -0.011 & -0.016 & 0.012 & -0.006 & 0.008 & -0.035 \\
0.031 & 0.002 & -0.006 & -0.011 & -0.003 & -0.007 & -0.038 & -0.002 \\
0.011 & 0.012 & -0.026 & -0.023 & 0.019 & 0.003 & 4.676e-4 & 0.010 \\
0.004 & -0.014 & 5.390e-4 & 0.028 & 0.010 & 0.032 & -0.008 & -0.003 \\
0.013 & -0.028 & -0.008 & -0.016 & 0.004 & -0.014 & -6.320e-4 & 0.013 \\
67.25 & 8.587 & 199.0 & 1130 & 178.6 & -45.37 & -47.35 & 28.89 \\
1734 & 67.15 & 1591 & 1971 & -31.48 & 1148 & 101.2 & 383.0 \\
52.76 & 32.48 & 67.13 & 102.1 & -17.85 & 76.92 & 106.4 & 199.3 \\
-11.21 & -18.51 & 37.07 & 3.593 & 20.87 & -34.99 & -34.81 & -57.68 \\
-8.847 & 2.283 & -7.036 & -21.20 & -7.391 & -23.20 & -5.618 & -20.02 \\
-0.547 & 1.925 & -2.516 & -1.299 & -0.071 & 0.667 & -0.652 & -1.496
\end{matrix}\right.
$$

$$
\left.\begin{matrix}
-3.296e-4 & 0.001 & -1.924e-4-8.704e-4i & -1.924e-4+8.704e-4i \\
-3.775e-4 & 7.649e-5 & -2.777e-4+1.070e-4i & -2.777e-4-1.070e-4i \\
7.160e-5 & -8.586e-6 & -6.143e-4-4.063e-4i & -6.143e-4+4.063e-4i \\
4.406e-4 & 0.001 & 3.791e-4+6.368e-4i & 3.791e-4-6.368e-4i \\
-8.249e-4 & 0.001 & -7.371e-5+1.795e-4i & -7.371e-5-1.795e-4i \\
-0.002 & -5.685e-4 & 2.168e-4+2.128e-4i & 2.168e-4-2.128e-4i \\
0.008 & -0.024 & 0.018+0.015i & 0.018-0.015i \\
0.009 & -0.002 & 0.004-0.007i & 0.004+0.007i \\
-0.001 & 1.803e-4 & 0.019-0.002i & 0.019+0.002i \\
-0.010 & -0.029 & -0.002-0.007i & -0.002-0.007i \\
0.019 & -0.026 & -0.001-0.005i & -0.001+0.005i \\
0.036 & 0.012 & -0.008-0.001i & -0.008+0.001i \\
-44.16 & 162.8 & -146.4+7.213i & -146.4-7.213i \\
-82.74 & 0.585 & -1.206+159.2i & -1.206-159.2i \\
-37.35 & -21.81 & -780.8+102.0i & -780.8-102.0i \\
9.782 & 55.18 & 10.56-30.61i & 10.56+30.61i \\
-2.507 & 12.38 & 13.80-9.295i & 13.80+9.295i \\
-1.510 & -2.249 & 0.712-0.682i & 0.712+0.682i
\end{matrix}\right]
$$

Box II

Table 4. Dynamic performance of external wrenches with the sinusoidal disturbance.

	Torque fluctuation					
Controller	$\Delta\bar{Q}_1$(NM)	$\Delta\bar{Q}_2$ (NM)	$\Delta\bar{Q}_3$ (NM)	$\Delta\bar{Q}_4$ (NM)	$\Delta\bar{Q}_5$ (NM)	$\Delta\bar{Q}_6$ (NM)
PI	153.7	402.3	242.6	98.7	222.5	70.8
ILQ	6.42	2.83	1.97	0.98	0.72	0.0018

the response parameters of PI controller cannot satisfy the basic requirements of dynamic response for the SCRM system for carving detailed structures in stone-carving. For the ILQ controller, the response time of each joint angle is only 0.005 s, the overshoot is only 0.51%, and every dynamic response parameter can satisfy the requirements of the dynamic parameters of SCRM system machining because the suitable closed-loop poles are selected in the process of designing the controller. In brief, the ILQ controller enjoys better control accuracy and set point tracking performance than the PI controller.

6.2. Disturbance rejection performance comparison

Because of the hardness and brittleness of stones and the flaws of natural crystallization, SCRM systems can be quite easily disturbed by load force and mutation of moment of force while carving stones. In particular, when carving detailed structures of stones, the load force and mutation of moment of force will eventually lead to wreckage of stone blanks, scrapping workpieces. To compare the disturbance rejection performance of the PI controller and the ILQ controller, a sinusoidal testing signal with an amplitude of 100 Nm and a cycle of 0.05 s was added to the external wrench at $t = 0.2$ s and the simulation results are shown in Figure 9.

The torque fluctuation range of joint $\Delta\bar{Q}_i$, which is the difference between the maximum and minimum values of the PI controller and ILQ controller, was calculated and the results are presented in Table 4.

As shown in Table 4, when the SCRM system encounters disturbance in the external wrench, there is substantial torque fluctuation in each joint. The

$$\mathbf{T}_1 = [\mathbf{t}_1, \mathbf{t}_2, \cdots, \mathbf{t}_n], \qquad \mathbf{G} = [\mathbf{g}_1, \mathbf{g}_2, \cdots, \mathbf{g}_n]$$

$$\mathbf{T}_1 = \begin{bmatrix}
4.037e-4 & 8.125e-5 & 7.065e-5 & 5.069e-4 & 0.001 & -2.920e-4 & -2.605e-4 & -5.511e-5 \\
0.002 & 2.017e-4 & 4.045e-4 & 7.469e-4 & -5.013e-4 & 2.302e-4 & -3.057e-4 & 0.001 \\
-0.001 & -7.120e-5 & 2.113e-4 & 4.870e-4 & 1.204e-4 & 2.525e-4 & 0.002 & 6.903e-5 \\
-5.352e-4 & -4.247e-4 & 9.116e-4 & 0.001 & -8.036e-4 & -9.413e-5 & -1.870e-5 & -3.909e-4 \\
-1.810e-4 & 4.715e-4 & -1.925e-5 & -0.001 & -4.309e-4 & -0.001 & 3.229e-4 & 1.036e-4 \\
-6.283e-4 & 9.783e-4 & 2.918e-4 & 7.052e-4 & -1.599e-4 & 5.019e-4 & 2.528e-5 & -4.822e-4 \\
-0.008 & -0.002 & -0.020 & -0.011 & -0.033 & 0.008 & 0.007 & 0.001 \\
-0.034 & -0.006 & -0.011 & -0.016 & 0.012 & -0.006 & 0.008 & -0.035 \\
0.031 & 0.002 & -0.006 & -0.011 & -0.003 & -0.007 & -0.038 & -0.002 \\
0.011 & 0.012 & -0.026 & -0.023 & 0.019 & 0.003 & 4.676e-4 & 0.010 \\
0.004 & -0.014 & 5.390e-4 & 0.028 & 0.010 & 0.032 & -0.008 & -0.003 \\
0.013 & -0.028 & -0.008 & -0.016 & 0.004 & -0.014 & -6.320e-4 & 0.013
\end{matrix}$$

$$\begin{matrix}
-3.296e-4 & 0.001 & -1.924e-4-8.704e-4i & -1.924e-4+8.704e-4i \\
-3.775e-4 & 7.649e-5 & -2.777e-4+1.070e-4i & -2.777e-4-1.070e-4i \\
7.160e-5 & -8.586e-6 & -6.143e-4-4.063e-4i & -6.143e-4+4.063e-4i \\
4.406e-4 & 0.001 & 3.791e-4+6.368e-4i & 3.791e-4-6.368e-4i \\
-8.249e-4 & 0.001 & -7.371e-5+1.795e-4i & -7.371e-5-1.795e-4i \\
-0.002 & -5.685e-4 & 2.168e-4+2.128e-4i & 2.168e-4-2.128e-4i \\
0.008 & -0.024 & 0.018+0.015i & 0.018-0.015i \\
0.009 & -0.002 & 0.004-0.007i & 0.004+0.007i \\
-0.001 & 1.803e-4 & 0.019-0.002i & 0.019+0.002i \\
-0.010 & -0.029 & -0.002-0.007i & -0.002-0.007i \\
0.019 & -0.026 & -0.001-0.005i & -0.001+0.005i \\
0.036 & 0.012 & -0.008-0.001i & -0.008+0.001i
\end{bmatrix}$$

$$\mathbf{G} = \begin{bmatrix}
67.25 & 8.587 & 199.0 & 1130 & 178.6 & -45.37 & -47.35 & 28.89 & -44.16 & 162.8 \\
1734 & 67.15 & 1591 & 1971 & -31.48 & 1148 & 101.2 & 383.0 & -82.74 & 0.585 \\
52.76 & 32.48 & 67.13 & 102.1 & -17.85 & 76.92 & 106.4 & 199.3 & -37.35 & -21.81 \\
-11.21 & -18.51 & 37.07 & 3.593 & 20.87 & -34.99 & -34.81 & -57.68 & 9.782 & 55.18 \\
-8.847 & 2.283 & -7.036 & -21.20 & -7.391 & -23.20 & -5.618 & -20.02 & -2.507 & 12.38 \\
-0.547 & 1.925 & -2.516 & -1.299 & -0.071 & 0.667 & -0.652 & -1.496 & -1.510 & -2.249
\end{matrix}$$

$$\begin{matrix}
-146.4+7.213i & -146.4-7.213i \\
-1.206+159.2i & -1.206-159.2i \\
-780.8+102.0i & -780.8-102.0i \\
10.56-30.61i & 10.56+30.61i \\
13.80-9.295i & 13.80+9.295i \\
0.712-0.682i & 0.712+0.682i
\end{bmatrix}.$$

Box III

$$\mathbf{K}_{F0} = \begin{bmatrix}
1.039e4 & 5.764e3 & 4.307e3 & 2.443e3 & 1.455e3 & -770.3 & 268.9 & 55.42 & 9.103 & 43.55 & -5.071 & -1.292 \\
-1.581e3 & 2.226e4 & 1.216e4 & -395.6 & 955.4 & 86.08 & 55.41 & 403.8 & 202.3 & -46.92 & -21.02 & -1.441 \\
-2.299e3 & 1.163e4 & 9.065e3 & -773.2 & 513.9 & -58.60 & 9.103 & 202.3 & 157.9 & -39.77 & -15.25 & -1.245 \\
2.724e3 & -2.538e3 & -1.997e3 & 2.082e3 & 99.48 & -150.9 & 43.55 & -46.92 & -39.77 & 48.96 & 7.407 & -1.705 \\
124.0 & -1.317e3 & -1.049e3 & 235.0 & 786.8 & 51.48 & -5.071 & -21.02 & -15.25 & 7.407 & 20.05 & -0.046 \\
-40.49 & -85.20 & -75.80 & -93.50 & -8.89 & 99.92 & -1.292 & -1.441 & -1.245 & -1.705 & -0.046 & 1.936
\end{bmatrix},$$

$$\mathbf{K}_{I0} = \begin{bmatrix}
9.324e4 & 1.112e5 & 1.028e5 & 2.933e4 & 3.877e4 & -2.030e4 \\
-7.049e4 & 3.037e5 & 1.782e5 & 1.527e4 & 3.647e4 & 806.1 \\
-6.057e4 & 1.645e5 & 1.285e5 & 2.999e3 & 2.212e4 & -2.119e3 \\
3.999e4 & -3.408e4 & -2.522e4 & 2.145e4 & -2.174e3 & -2.399e3 \\
5.875e3 & -1.989e4 & -1.678e4 & 1.608e3 & 7.068e3 & 1.533e3 \\
-212.7 & -1.231e3 & -1.119e3 & -1.228e3 & -188.7 & 1.284e3
\end{bmatrix}.$$

Box IV

torque fluctuation ranges of joints 2 and 3 given by the PI controller reach 402.3 Nm and 242.6 Nm, respectively, which are unacceptable for the SCRM system. Given that the optimization and feedback correction strategies were designed using the ILQ controller, the disturbances can be corrected rapidly and the torque fluctuation in all joints is controlled in a small region. Hence, the ILQ controller can increase the disturbance rejection performance of the SCRM system.

6.3. Robustness performance comparison

The basic dynamic characteristic parameters of the SCRM system are changed with the actuator state,

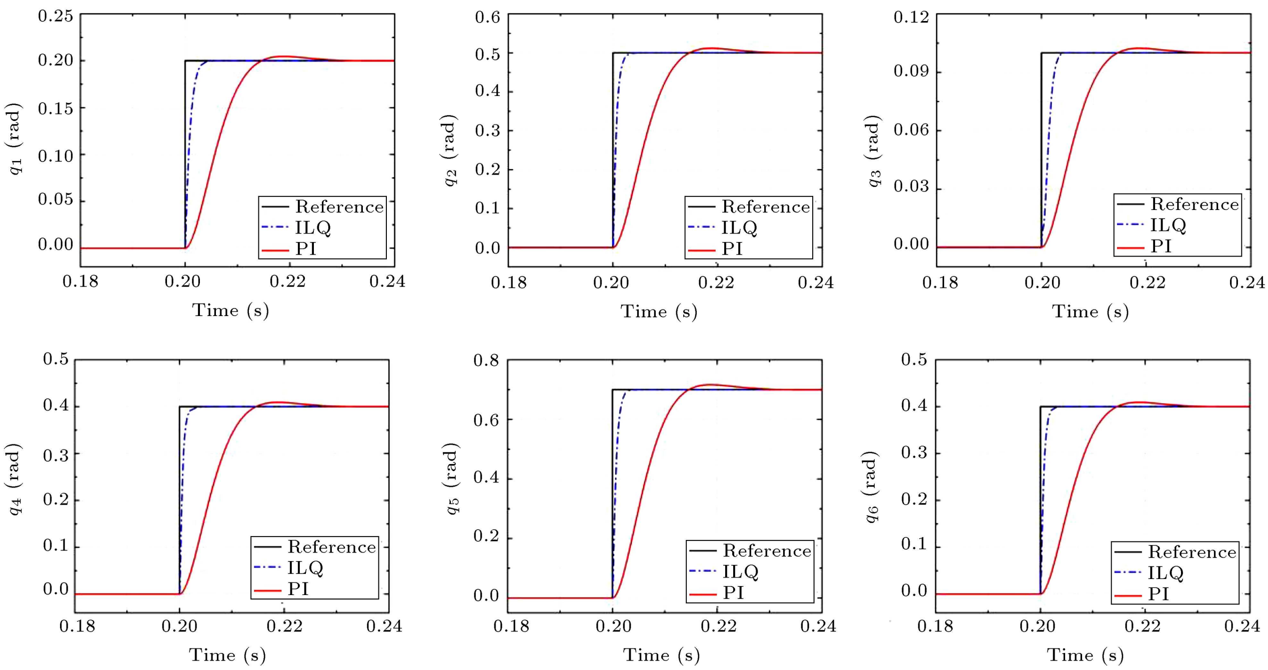

Figure 8. Comparison of the step responses of PI and ILQ at joint angles 1 to 6 of the SCRM system.

Table 5. Dynamic performance as the moment of inertia changes.

Torque fluctuation	Moment of inertia							
	Change=200%		Change=400%		Change=600%		Change=700%	
	PI	ILQ	PI	ILQ	PI	ILQ	PI	ILQ
$\Delta\bar{Q}_1$ (Nm)	183.2	41.3	208.5	42.1	214.9	42.9	227.8	43.1
$\Delta\bar{Q}_2$ (Nm)	488.7	137.1	536.9	137.5	563.3	138.1	587.2	138.6
$\Delta\bar{Q}_3$ (Nm)	301.9	65.1	342.2	65.4	353.3	65.8	375.5	66.3
$\Delta\bar{Q}_4$ (Nm)	89.7	23.4	99.3	23.8	105.8	24.2	115.7	24.8
$\Delta\bar{Q}_5$ (Nm)	311.3	58.3	354.8	58.7	375.3	59.2	398.2	59.8
$\Delta\bar{Q}_6$ (Nm)	85.5	1.68	98.6	1.72	105.3	1.79	113.4	1.83

joint damping, and environment temperature variation. In addition, the model mismatch caused by the change in the dynamic parameters substantially affects the dynamic performance of the SCRM system. To study the robustness of the PI controller and the ILQ controller, the dynamic performances of both controllers were simulated under the condition that the moment of inertia and link mass might change. Under the condition that the moment of inertia changes from 100% to 700%, a testing track signal, shown in Eq. (52), was added to the initial value of the joint position vector, joint velocity vector, and joint acceleration vector at $t = 0.2$ s. The simulation results are shown in Figure 10.

$$\begin{cases} \mathbf{q}(t) = a + bt + ct^2 + dt^3 + mt^4 + nt^5 \\ \dot{\mathbf{q}}(t) = b + 2ct + 3dt^2 + 4mt^3 + 5n^4 \\ \ddot{\mathbf{q}}(t) = 2c + 6dt + 12mt^2 + 20n^3 \end{cases} \tag{52}$$

where $a = \theta_0$, $b = c = 0$, $d = 10\theta_{tf}$, $m = -7.5\theta_{tf}$, and $n = 1.5\theta_{tf}$.

$$\theta_{tf} = \begin{bmatrix} \frac{pi}{4} & \frac{2pi}{3} & \frac{pi}{8} & \frac{pi}{2} & \frac{5pi}{6} & \frac{pi}{2} \end{bmatrix},$$

$$\theta_0 = \begin{bmatrix} 0 & 0 & 0 & 0 & 0 & 0 \end{bmatrix}.$$

The torque fluctuation range of joint $\Delta\bar{Q}_i$, which is the difference between the maximum and minimum values of the PI controller and the ILQ controller, was calculated and the results are presented in Table 5.

Based on the simulation results presented above, when the moment of inertia or link mass changes, the robustness of the PI controller decreases and then, a large joint torque fluctuation range or fluctuation time appears. However, the SCRM system based on the proposed ILQ controller is relatively insensitive to the dynamic characteristic parameter changes and model mismatch. When a testing track signal was added

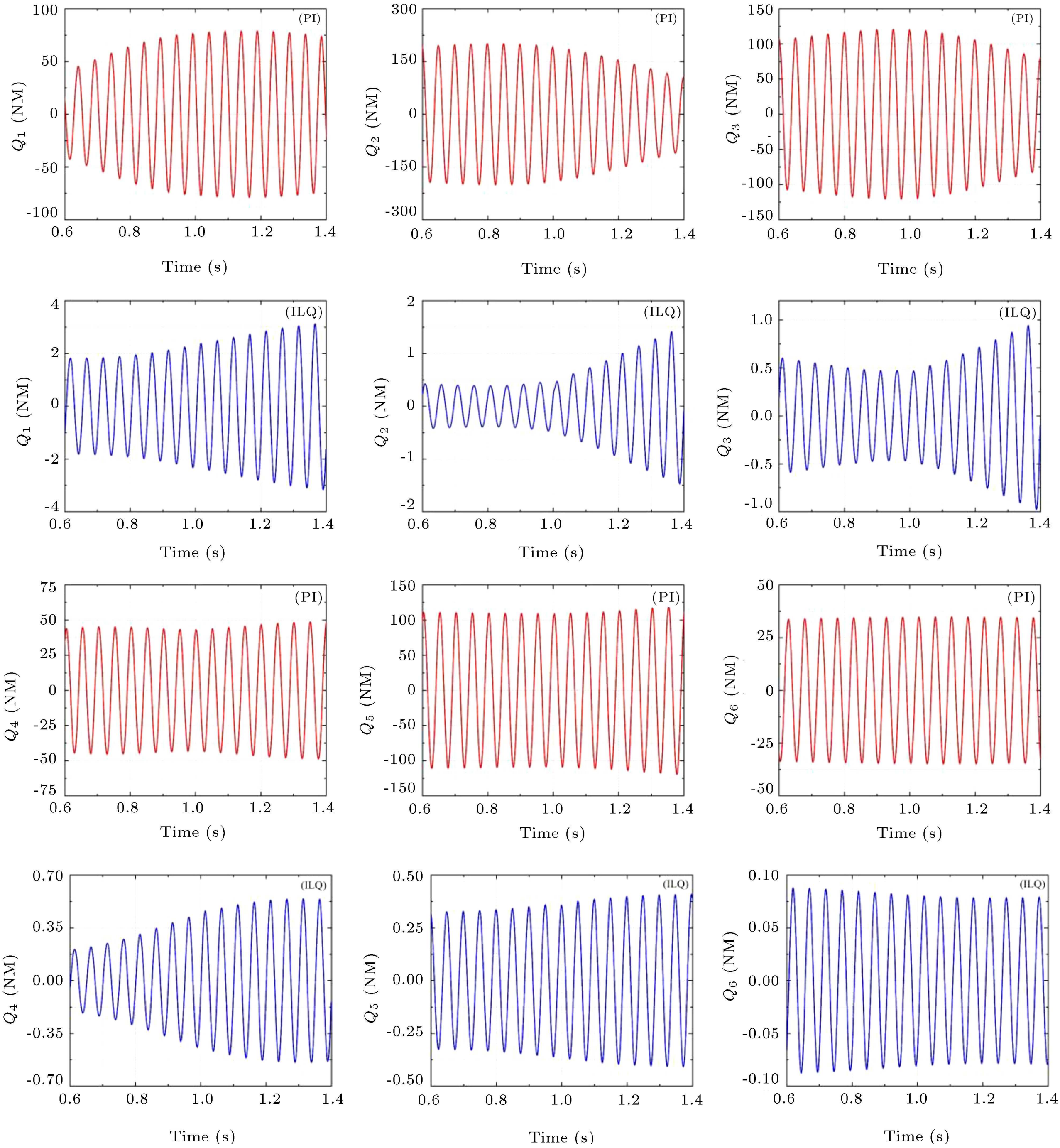

Figure 9. Comparison of the sinusoidal disturbance in external wrenches of PI and ILQ at joint angles 1 to 6 of the SCRM system.

to the initial value of the joint angle vector, joint velocity vector, and joint acceleration vector, the PI controller had a torque fluctuation range of 587.6 Nm at joint 2, while the proposed ILQ controller had a torque fluctuation range of only 138.6 Nm at joint 2. The results presented above clearly show that compared to the PI controller, the ILQ controller is more robust and provides better control effect for the SCRM system.

7. Conclusions

In this paper, an optimal control scheme was designed based on Inverse Linear Quadratic (ILQ) theory for an Stone-Carving Robotic Manipulator (SCRM) system. First, the dynamic equation and state-space model of the SCRM system were established by the Lagrange method. The ILQ controller, which combined simplicity and effectiveness, was designed for the established

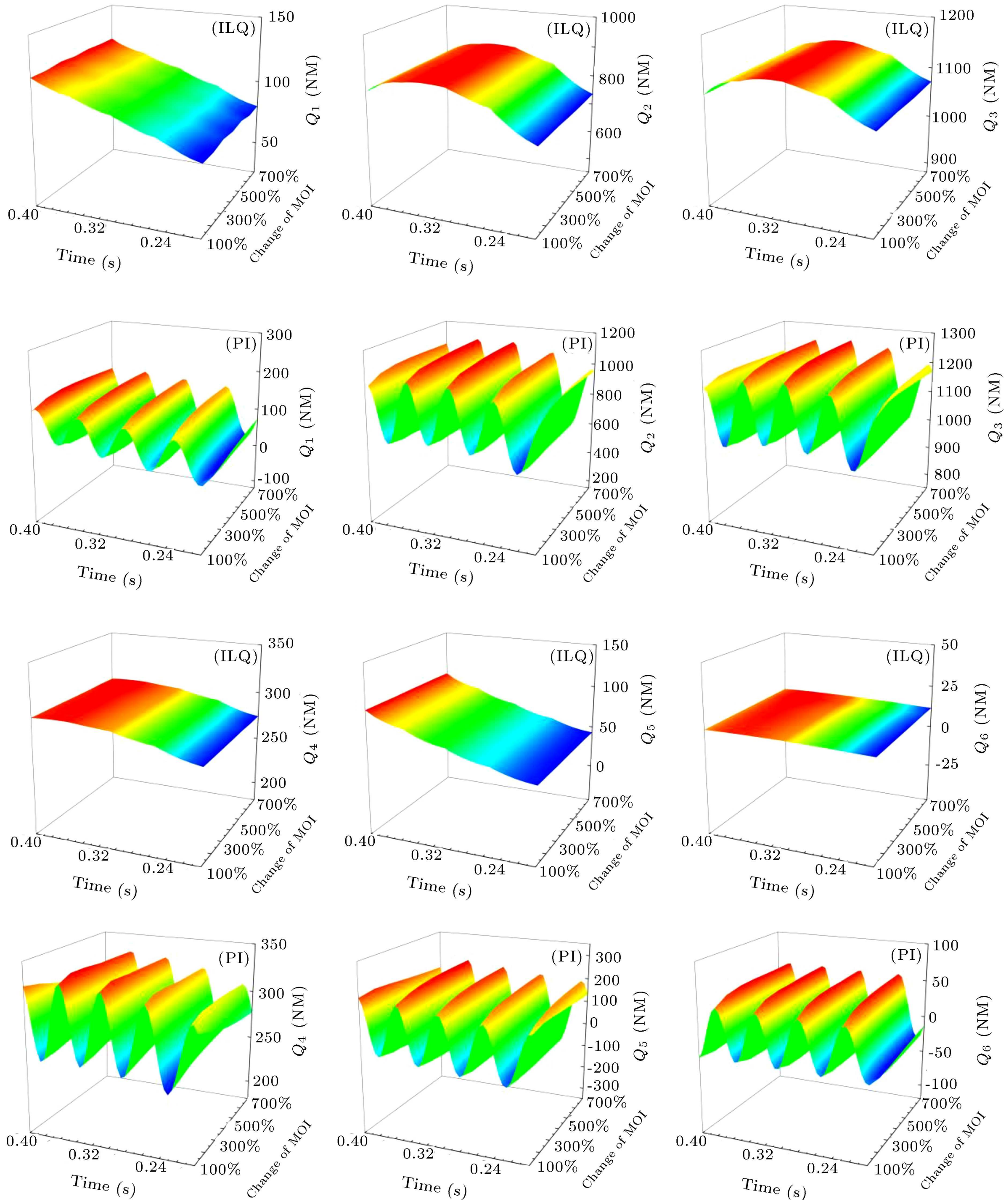

Figure 10. Comparison of changing the moment of inertia of PI and ILQ at joint torques 1 to 6 of the SCRM system.

model and according to the desired dynamic and steady performance, the joint angle and joint torque of the SCRM system were controlled through the desired closed-loop pole assignment and tuning of the weighting matrices.

The control performance of the proposed ILQ controller was compared with that of the PI controller. For the ILQ controller, the rising time and overshoot of the joint angle were 0.005 s and 0.51%, respectively, and the dynamic performance was much better than that of the PI controller. Considering the external wrench disturbances as well as the moment of inertia or link mass changes, good control performances including strong disturbance rejection and perfect robust stability can be obtained in the SCRM system by the ILQ controller. Simulation results pointed to the higher effectiveness of the proposed SCRM control scheme than the traditional control strategies. With the help of the powerful computing capacity of the programmable logic controller and the experience of the ILQ controller in the SCRM system, the ILQ control theory is a good prospect for use in other fields of automation and industrial control. In the future works, the dynamic model with uncertainties will be further considered, while the neural network or learning control can be employed to approximate the dynamic model of SCRM system. Then, in order to improve the response speed and tracking accuracy of SCRM, the RBFNN-based ILQ control strategy will be designed for SCRM.

Acknowledgment

This work was supported by National Natural Science Foundation of China (Grant#51905181) and Natural Science Foundation of Fujian Province (Grant#2019J01084). The authors would like to thank the sponsor for this support. YFC would acknowledge the support from the "Promotion Program for Young and Middle-aged Teacher in Science and Technology Research of Huaqiao University".

References

1. Lu, L., Zhang, J., Han, J., et al. "Time-optimal tool motion planning with tool-tip kinematic constraints for robotic machining of sculptured surfaces", *Robotics and Computer-Integrated Manufacturing*, **65**, p. 101969 (2020).
2. Andersson, J.E. and Johansson, G. "Robot control for wood carving operations", *Mechatronics*, **11**, pp. 475–490 (2001).
3. Yin, F.C., Ji, Q.Z., and Wang, C.Z. "Research on machining error prediction and compensation technology for a stone-carving robotic manipulator", *International Journal of Advanced Manufacturing Technology*, **115**, pp. 1683–1700 (2021).
4. Yin, F.C., Ji, Q.Z., and Jin, C.W. "An improved QPSO-SVM-based approach for predicting the milling force for white marble in robot stone machining", *Journal of Intelligent & Fuzzy Systems*, **41**, pp. 1589–1609 (2021).
5. Wen, S.H., Zheng, W., Jia, S.D., et al. "Unactuated force control of 5-DOF parallel robot based on fuzzy PI", *International Journal of Control, Automation and Systems*, **18**(6), pp. 1629–1640 (2020).
6. Garrido, R. and Trujano, M.A. "Stability analysis of a visual PID controller applied to a planar robot", *International Journal of Control, Automation and Systems*, **17**(6), pp. 1589–1598 (2019).
7. Su, Y.X., Sun, D., and Duan, B.Y. "Design of an enhanced nonlinear PID controller", *Mechatronics*, **15**(8), pp. 1005–1024 (2005).
8. Van, M., Do, X.P., and Mavrovouniotis, M. "Self-tuning PID-nonsingular fast terminal sliding mode control for robust fault tolerant control of robot manipulators", *ISA Transactions*, **96**, pp. 60–68 (2020).
9. Nohooji, H.R. "Constrained neural adaptive PID control for robot manipulators", *Journal of the Franklin Institute*, **357**(7), pp. 3907–3923 (2020).
10. Huang, H., Zhang, T., and Yang, C. "Motor learning and generalization using broad learning adaptive neural control", *IEEE Transactions on Industrial Electronics*, **67**, pp. 8608–8617 (2020).
11. Liu, C.X., Wen, G.L., Zhao, Z.J., et al. "Modeling, control, and simulation of a SCARA PRR-type robot manipulator", *IEEE Transactions on Cybernetics*, **99**, pp. 1–8 (2020).
12. He, W. and Dong, Y.T. "Adaptive fuzzy neural network control for a constrained robot using impedance learning", *EEE Transactions on Neural Networks and Learning Systems*, **29**(4), pp. 1174–1186 (2018).
13. Zhang, T., Wang, X., Xu, X., et al. "GCB-Net: Graph convolutional broad network and its application in emotion recognition", *IEEE Transactions on Affective Computing*, **13**(1), pp. 379–388 (2019).
14. Li, C.G., Cui, W., Yan, D.D., et al. "Adaptive dynamic surface control of a flexible-joint robot with parametric uncertainties", *Scientia Iranica*, **26**(5), pp. 2749–2759 (2019).
15. He, W., Dong, Y., and Sun, C. "Adaptive neural impedance control of a robotic manipulator with input saturation", *IEEE Transactions on Systems Man Cybernetics-Systems*, **46**, pp. 334–344 (2016).
16. Chen, W. and Jiao, L. "Adaptive tracking for periodically time-varying and nonlinearly parameterized systems using multilayer neural networks", *IEEE Transactions on Neural Networks and Learning Systems*, **21**(2), pp. 345–351 (2010).
17. Talole, S.E., Kolhe, J.P., and Phadke, S.B. "Extended-state-observer-based control of flexible-joint system with experimental validation", *IEEE Transactions on Industrial Electronics*, **57**(4), pp. 1411–1419 (2010).
18. Liu, Y., Liu, H., and Meng, Y.N. "Active disturbance rejection control for a multiple-flexible-link manipulator", *Journal of Harbin Institute of Technology*, **25**(1), pp. 18–28 (2018).
19. Saeed, A. and Barjuei, E.S. "Linear quadratic optimal controller for cable-driven parallel robots", *Frontiers of Mechanical Engineering*, **10**, pp. 344–351 (2014).
20. Pan, H.J. and Xin, M. "Nonlinear robust and optimal control of robot manipulators", *Nonlinear Dynamics*, **76**, pp. 237–254 (2014).
21. Zhang, H., Umenberger, J., and Hu, X.M. "Inverse optimal control for discrete-time finite-horizon linear quadratic regulators", *Automatica*, **110**, p. 108593 (2019).
22. Li, Y.B., Yao, Y., and Hu, X.M. "Continuous-time inverse quadratic optimal control problem", *Automatica*, **117,** p. 108977 (2020).

23. Xu, J.Y., Liu, H.P., and Zhou, J.H. "Tracking robustness of model-reference inverse linear quadratic (MR-ILQ) optimal current-control for permanent magnet synchronous motor", *Control Theory & Applications*, **25**(6), pp. 1081–1084 (2008).
24. Hu, Y.J., Sun, J., Wang, Q.L., et al. "Characteristic analysis and optimal control of the thickness and tension system on tandem cold rolling", *International Journal of Advanced Manufacturing Technology*, **101**, pp. 2297–2312 (2019).
25. Liu, C.X., Zhao, Z.J., and Wen, G.L. "Adaptive neural network control with optimal number of hidden nodes for trajectory tracking of robot manipulators", *Neurocomputing*, **350**, pp. 60–68 (2019).
26. Van, M., Do, X.P., and Mavrovouniotis, M. "Self-tuning PID-nonsingular fast terminal sliding mode control for robust fault tolerant control of robot manipulators", *ISA Transactions*, **96**, pp. 60–68 (2019).
27. Wang, G.C., Wang, W.C., and Yan, Z.G. "Linear quadratic control of backward stochastic differential equation with partial information", *Applied Mathematics and Computation*, **403**, p. 126164 (2021).
28. Yu, C.P., Li, Y., and Fang, H. "System identification approach for inverse optimal control of finite-horizon linear quadratic regulators", *Automatica*, **129**, p. 109636 (2021).

Biographies

Fangchen Yin received the BSc degree in Material Processing from Shenyang University of Technology, China and the MSc and PhD degrees in Material Processing from the Northeastern University, China in 2013 and 2017, respectively. He is currently a Lecturer at the HuaQiao University. He has been involved in developing, designing, and commissioning of various areas of several robotic machining projects.

Yanwen Jun received the B.S.E. degree in Mechanical Manufacturing from HuaQiao University, China in 2019 and was awarded the first-class scholarship of Huaqiao University and the title of Outstanding Graduate of Huaqiao University. He is currently a Master graduate student at the HuaQiao University. He is currently working on modern control theory.